Aeroacoustics Conferences
30 May - 1 June, 2016, Lyon, France
22nd AIAA/CEAS Aeroacoustics Conference





# Tonal dynamics and sound in free and installed turbulent jets

V. Jaunet & P. Jordan
*Institut Pprime, CNRS-Université de Poitiers-ENSMA, Poitiers, France*

A. V. G. Cavalieri
*Instituto Tecnológico de Aeronáutica, São José dos Campos, Brazil*

A. Towne, T. Colonius & O. Schmidt
*California Institute of Technology, Pasadena, CA, USA*

G. A. Brès
*Cascade Technologies Inc., Palo Alto, CA, USA*



**Acoustic waves trapped in the potential core of subsonic turbulent jets have recently been observed and explained by Towne *et al.*[11,13,14] We show that these waves also radiate outside the jet, primarily into the upstream arc. We provide an experimental identification of the Mach-number dependence of the phenomenon, which indicates that the modes are active even when evanescent, probably due to turbulent forcing. Finally, we show that for Mach numbers lower than about 0.8, the strong tonal dynamics and sound radiation (up to 170dB) that occur when a sharp edge is placed close to the jet are related to a resonance mechanism involving convective hydrodynamic wavepackets and a 'slow', upstream-propagating, trapped acoustic mode. A Helmholtz scaling of the resonance at higher Mach number suggests involvement of the 'fast' trapped modes in the range $0.8 \leq M \leq 1$.**

## I. Introduction

It is generally accepted that subsonic turbulent jets are amplifier flows, with broadband dynamics, and, consequently, broadband sound radiation, as opposed to oscillator flows, such as the cylinder wake, which are dominated by dynamics with well-defined frequencies.[7] But a number of recent studies have shown that under certain conditions jets can support tonal dynamics. Suzuki & Colonius[12] observed what they assumed were spurious discrete spectral peaks in nearfield measurements and attributed them to pipe modes upstream of the nozzle exit plane. Motion pictures from large eddy simulations frequently reveal organised waves, with upstream phase velocity, within the potential core. Lawrence & Self[8] have measured tonal sound radiation from turbulent jets when a sharp edge (trailing edge of a wing model for instance) is situated close to the jet. Zaman *et al.*[15] have found that the presence of a flat plate in the nearfield of a rectangular jet can lead to tonal dynamics.

Recent studies by Towne *et al.*[13,14] and Schmidt *et al.*[11] have revisited the tones observed by Suzuki & Colonius.[12] Figure 1(a) shows pressure spectra (black from experiment, blue from Large Eddy Simulation) in the near-nozzle region of a turbulent jet at Mach 0.9. Figure 1(b), which presents a frequency-wavenumber transform of the pressure (from LES) on the jet centerline, shows that the peaks observed in the near-nozzle pressure spectra are associated with perturbations whose phase velocity is negative. A theoretical analysis, discussed briefly in the next section, shows that these traits are due to trapped acoustic waves that experience the shear-layer as a pressure-release surface.

Whether or not these trapped waves are dynamically or acoustically important remains to be established, and it is this question that motivates the work we present here. A series of experiments are performed for both free jets and jets with a flat plate edge situated in the nearfield. The Mach number of the flow is varied and microphone measurements performed in the near-nozzle region in order to record the signature

of the 'trapped' waves, as per Towne *et al.*,[13,14] and in the acoustic field using both azimuthal and polar microphone arrays.

The study establishes: (1) that the 'trapped' waves of Towne *et al.*[13,14] and Schmidt *et al.*[11] do radiate to the farfield, the signature being clearest at high polar angles ($\theta > 90°$) in free-jet conditions; (2) that strong tones observed in the acoustic field when a sharp edge is introduced to the nearfield (as per Lawrence & Self[8]) are associated with these trapped waves; (3) that the presence of the edge can cause the jet to behave as an oscillator rather than an amplifier (i.e. the flow exhibits traits of global rather than convective instability), acoustic tones of up to 170dB being produced.

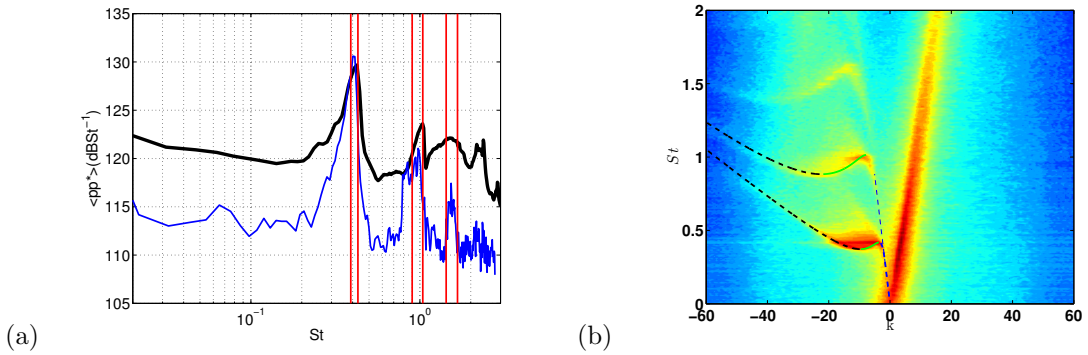


**Figure 1. (a) Pressure spectra of azimuthal mode, $m = 0$, in near-nozzle region, $(x/D, r/D) = (0.1, 0.6)$; black: experiment; blue: LES; (b) frequency-wavenumber spectrum of $m = 0$ pressure at $r/D = 0$ from LES.**

## II. Theory

Towne *et al.*[13,14] have shown that the tones manifest in figure 1 are associated with eigenmodes of a cylindrical vortex sheet, which are solutions of the dispersion relation,[9]

$$\mathcal{D}_j(M,\omega,k) = \frac{1}{(1-\frac{kM}{\omega})^2} + \frac{\Phi K_m'(k\Phi) I_m(k\Psi)}{\Psi K_m(k\Phi) I_m'(k\Psi)}, \tag{1}$$

where

$$\Phi = \sqrt{1-\left(\frac{\omega}{k}\right)^2} \quad , \quad \Psi = \sqrt{1-\left(M-\frac{\omega}{k}\right)^2}, \tag{2}$$

$M$, $\omega$ and $k$ are, respectively, the Mach number, Helmholtz number and streamwise wavenumber, and $I_m$ and $K_m$ are the modified Bessel functions of the first and second kind.

A criterion can be obtained that determines the conditions under which acoustic duct modes approximately solve the vortex-sheet problem by substituting into equation 1 an $(M,\omega,k)$ combination that satisfies the duct dispersion relation. For a soft-walled duct (zero impedance) the criterion is,

$$\left|1-\frac{kM}{\omega}\right|^2 \gg 1. \tag{3}$$

Figure 2 shows eigenspectra for vortex-sheet, rigid- and soft-walled ducts and a parallel jet whose shear layer has finite thickness. The inner and outer semi-circles correspond, respectively, to modes satisfying $|1-kM/\omega|^2$=1 & 10. At $St = 0.36$ (figure 2a) eigenvalues in the left half plane corresponding to the finite-thickness jet, vortex sheet and soft-walled duct almost coincide. At this frequency they are evanescent waves with negative phase-velocity and positive group velocity—a space-time stability analysis confirms that this is a $k^+$ branch. At $St = 0.4$ (figure 2b) the modes have cut on, and the cut-on point corresponds to a saddle point formed between the $k^+$ branch and its complex-conjugate, $k^-$, branch. For the vortex-sheet and parallel jet eigenvalues the cut-on saddle point is referred to as $s_1$, whereas the soft-walled duct saddle is denoted $s_d$ ($s_1$ and $s_d$ coincide when $|1-kM/\omega|^2 >> 1$).

As the frequency is increased further the duct eigenvalues continue their trajectory along the real axis, whereas the vortex-sheet and jet eigenvalues depart into the upper half plane just after crossing the outer

semicircle (i.e. they cease to behave like duct modes); the departure point corresponds to a second saddle point (which we will refer to as $s_2$), between the $k^+$ branch and another $k^-$ branch that originates from the upstream-acoustic-mode branch. The theoretical cut-on and cut-off frequencies are plotted as vertical red lines in figure 1(a) for the first, second and third radial modes. The eigenvalue trajectories are plotted in figure 1b: the green line corresponds to the $k^+$ branch discussed above; the dashed black and blue lines correspond to the two $k^-$ branches that form the saddle points, $s_1$ and $s_2$, with the $k^+$ branch as discussed. The eigenvalues shown in figure 1a are associated with azimuthal mode, $m = 0$ and radial mode, $n_r = 1$. While in theory an infinite number of $(m, n_r)$ modes exist, in this paper we focus primarily on $(m, n_r) = (0, 1)$ & $(1, 1)$.

As described in more detail in,[14] these propagative $k^+$ and $k^-$ modes enable the occurrence of resonance. Two kinds of resonance mechanism are possible: saddle-point resonance, which does not require "end conditions" and a second mechanism underpinned by "end conditions" provided by the nozzle on one hand, and by the change of the $k^+$ mode from propagative to evanescent (i.e. a turning point) upstream of the end of the potential core.

The theoretical Mach-number dependence of the saddle points $s_1$ and $s_2$ is shown in figure 3. For Mach numbers below $M = 0.82$, while the saddle points occur at the same real frequency, they move off the real wavenumber axis into the positive and negative half planes for $s_1$ and $s_2$ respectively, leaving only one $k^-$ branch on the real axis (i.e. there is now only one, rather than three, propagative modes). Furthermore, saddle-point $s_1$, which is formed between an evanescent $k^+$ and a propagative $k^-$ branch, now has negative imaginary frequency (i.e. is stable). This suggests that the resonance mechanisms evoked above should be disabled for $M < 0.82$.

These theoretical predictions will be compared with the experimental measurements in what follows, and will serve as a guide for understanding the physics of the tonal dynamics and sound observed in both the free and "installed" jets.

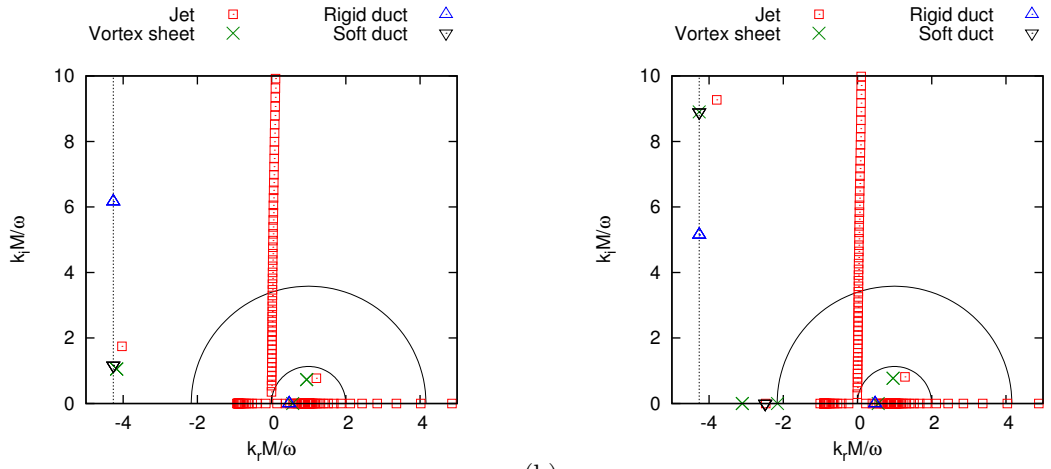


**Figure 2. Eigenspectra. (a)** $St = 0.36$**; (b) St=0.4.**

## III. Experiment

The experiments were performed in the *Bruit et Vent* anechoïc jet-noise facility of the PPRIME Institute, Poitiers, France. The anechoïc chamber has dimensions of $9.6m \times 6m \times 3.4m$, and is equipped with absorbing foam of depth 0.4 m. The cut-off frequency is 212 Hz. The nozzle, of diameter, $D = 0.05$ m, is the same used in a number of previous papers[1–6,10] where the flow and sound fields have been extensively studied in uninstalled and installed configurations for the Mach number range $0.4 \leq M \leq 0.9$.

In order to explore the behaviour of the 'trapped' waves and their sound radiation a total of 27 microphones were used. The microphone situated at $(x/D, z/D) = (0.04, 0.55)$ (cf. figure 4(b)) will be referred to as probe, $p_{TW}$, as it is at this position that the spectral signature of trapped waves (TW) is most clearly

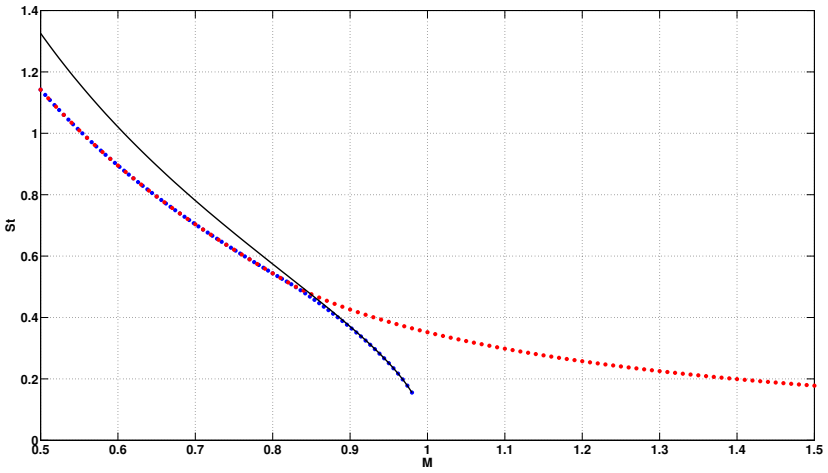


**Figure 3.** $M - St$ **dependence of saddle-points:** $s_1$ **(blue),** $s_2$ **(red) and** $s_d$ **(black)**

observed, as per figure 1(a). In addition to this microphone the azimuthal array shown in figure 4(a), of radius $14.3D$, was equipped with 18 microphones (to be referred to as probes $p_{\phi_1} : p_{\phi_{18}}$). For the free jet measurements this is situated at an axial position such that the microphones lie at polar angle, $\theta = 20°$. For the experiments with the flat plate, the axial position is such that the microphones lie in the plane containing the plate edge (position shown in figure 4(a)), in anticipation of the sound field produced when the nearfield pressure fluctuations are scattered by the edge. Finally, a polar array of microphones, in the $x - z$ plane as per figure 5, on the unshielded side of the installed configuration, comprised microphones from $\theta = 30°$ to $\theta = 100°$ in increments of $10°$ (these will be referred to as probes $p_{\theta_{10}} : p_{\theta_{100}}$). A final microphone, situated at $\theta = 140°$ and $R/D = 6$ and referred to as probe $p_{\theta_{140}}$, can be seen at the bottom of figure 4(b).

The experimental procedure involved changing the flow Mach number from $M = 1$ to $M = 0.6$, in increments of $M = 0.02$, and recording 20 seconds of data at $200kHz$ for each test point. Prior to each acquisition it was ensured that the flow was in an isothermal state, $T_s/T_a = 1$, to an accuracy of $\approx \pm 1°K$.

## IV. Results & discussion

### A. Free jet

The hydrodynamic and acoustic pressure fields associated with the free jet are first considered.

#### *1. Mach-number dependence*

The power spectral density of the pressure fluctuation measured by probe $p_{TW}$ is shown in figure 6 as a function of Mach number. The spectral peaks of figure 1(a) are again observed at $M = 0.9$; additional peaks associated with higher-order azimuthal and radial modes can also be observed (the peak at $St \approx 0.6$ for $M = 0.9$ for instance corresponds to azimuthal mode, $m = \pm 1$). Superposed on the map are circles corresponding to the red dots of figure 3, i.e. the evolution of saddle-point $s_2$ over the entire Mach-number range, and saddle-point $s_1$ over the range $0.6 < M < 0.82$. We see a close correspondance between the measured Mach-number dependence and the theoretical prediction for the saddle points. The result suggests that saddle-point $s_2$, which is a shear-layer, rather than duct, mode is the more important of the two where the tones are concerned.

#### *2. Forced resonance?*

The persistence of the peaks for $M < 0.82$, which is in contradiction with the theoretical prediction that resonance should be disabled at these lower Mach numbers, suggests the presence of another ingredient, not

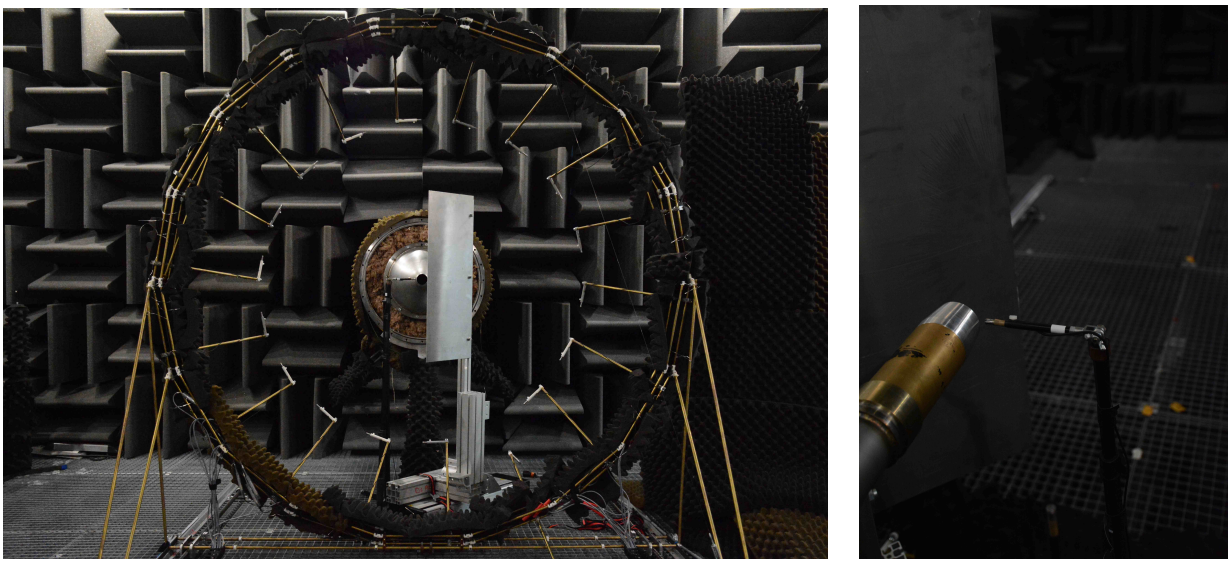

(a) (b)

**Figure 4. Experimental setup. (a) View from downstream; (b) View from behind the nozzle, showing microphone, $p_{TW}$.**

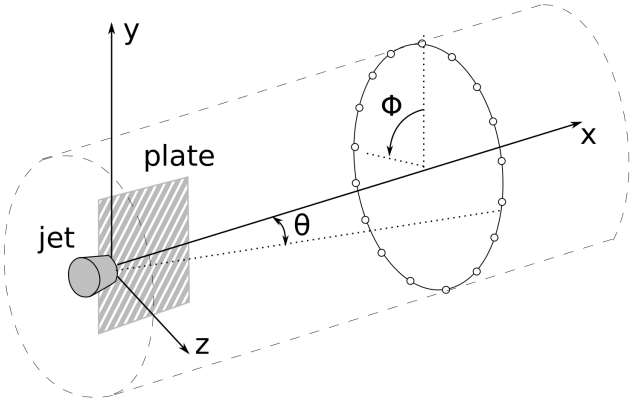


**Figure 5. Coordinate system.**

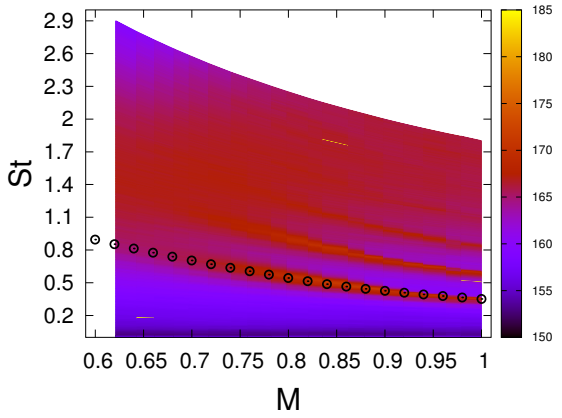


**Figure 6. Power spectral density, measured by microphone situated next to the nozzle lip, at $(x/D, r/D) = (0.04, 0.55)$, as a function of Mach number. Circles show the theoretical prediction for vortex-sheet saddle points for mode $(m, n_r) = (0, 1)$.**



included in the theoretical considerations discussed above: turbulence, which may provide a forcing of the modes sufficient for sustenance of the resonance mechanism despite the evanescent $k^+$ branch and the stable saddle point. The weakening of the spectral peaks as the Mach number decreases—and the saddle point becomes increasingly stable—is consistent with this idea. Further theoretical probing of the forced problem will require consideration in the resolvent framework.

### *3. Sound radiation*

Figure 7(a) shows the same PSD map, the overlayed dots now corresponding to lines proportional to $1/M^2$. This empirical law is found to capture the Mach-number dependence of all tones observed. Figure 7(b) shows a map of coherence between probes $p_{TW}$ and $p_{\theta_{100}}$. Coherence levels of up to 10% are seen to exist between trapped-wave modes $(0, 1)$ and $(1, 1)$ and the farfield sound at high polar angle. Smaller levels of coherence, $O(2\%)$, with a similar $1/M^2$ dependence can be observed at low polar angles (not shown here).

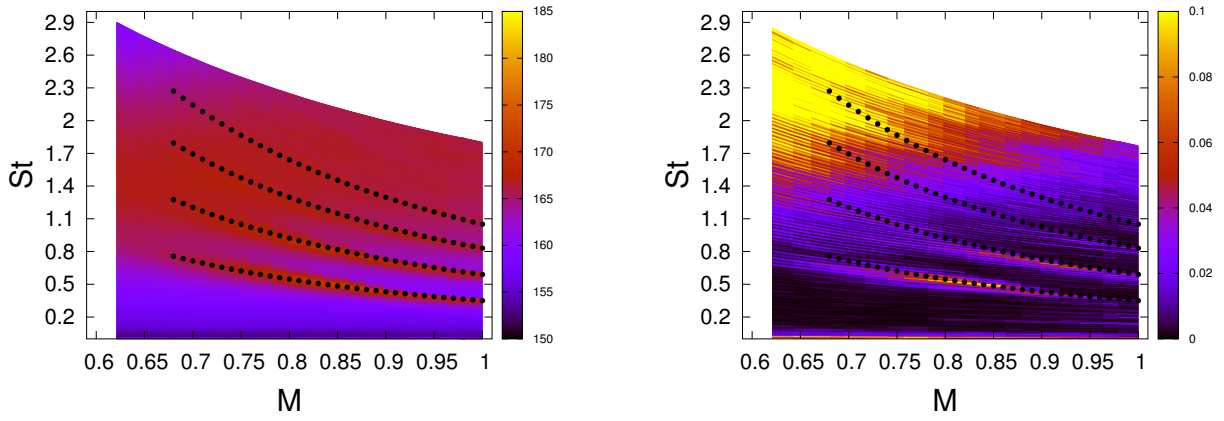


(a) (b)

**Figure 7. (a) Same data as figure 6 with lines proportional to $1/M^2$ superposed in order to highlight the signature of modes $(m, n_r) = (0, 1)$, $(1, 1)$, $(0, 2)$, $(1, 2)$ (from bottom to top); (b) Coherence between nearfield microphone (at $(x/D, r/D) = (0.04, 0.55)$) and microphone at radial distance, $r/D = 30$, and polar angle, $\theta = 100°$ (measured from the nozzle exit plane).**

This confirms that the so-called trapped waves leave their signature in the farfield; the radiation mechanism may involve diffraction by the nozzle lip. It is interesting that the highest coherence levels are observed at $M \approx 0.82$, which theory shows to corresponds to a double saddle point (cf. figure 3, where red and blue lines merge) on the real wavenumber axis.

## B. Jet with an edge in the nearfield

A rectangular aluminium plate was situated in the nearfield, inclined, in the $X - Z$ plane, toward the jet at 45°. With the trailing edge of the plate at $x/D = 2$ 'non-grazing' and 'grazing' radial positions were considered, respectively, $r/D = 0.8$ (mean flow is zero at this point) and $r/D = 0.5$ (the lip-line). We note that the former position is of some interest as flaps can protrude to this radial location for installed UHBR engines; in fact Lawrence & Self[8] have explored even higher-penetration configurations using a wing-model and a co-axial jet issuing from a nozzle with realistic industry lines; similar tones to those observed here occurred in that configuration. For two additional axial positions of the trailing edge, $x/D = 3$ and 4 only the grazing location was considered.

### 1. *Edge tones*

Figure 10 shows power spectral density of the pressure fluctuations measured by microphone $p_{TW}$ when the plate edge is at $r/D = 0.5$ and the streamwise position varied ($x/D = 2$, 3 & 4). A complex of strong tones is manifest; peak hydrodynamic SPL reaches $O(200dB)$ and the associated peak acoustic levels, at $r/D = 14.3$, $O(170dB)$. The spectral organisation of the peaks is a function of Mach number and streamwise position of the plate edge.

In order to identify the mechanisms responsible for the tones we must consider the four resonance possibilities that are enabled on account of both the three trapped waves discussed above and the Kelvin-Helmholtz mode. One should note that these resonance mechanisms differ from those associated with the turning point in so far as the plate edge can couple any combination of $k^+$ and $k^-$ modes, whereas, as discussed by Towne *et al.*,[14] where the intrinsic resonance mechanisms are concerned the turning points dictate which modes can be coupled.

A zoom taken from figure 1(b) is shown in figure 9. The dispersion relations of the four modes, shown by the blue line, are denoted as follows: $k^+_{KH}$ indicates the Kelvin-Helmholtz mode, associated with convected hydrodynamic wavepackets; $k^+_p$ and $k^-_p$ indicate the trapped waves that form saddle point, $s_2$ (where the blue line has zero slope and a local maximum); $k^-_d$ indicates the 'slow' duct mode, and which forms saddle point, $s_1$ (where the blue line has zero slope and a local minimum) with the 'fast' duct mode, $k^+_p$.

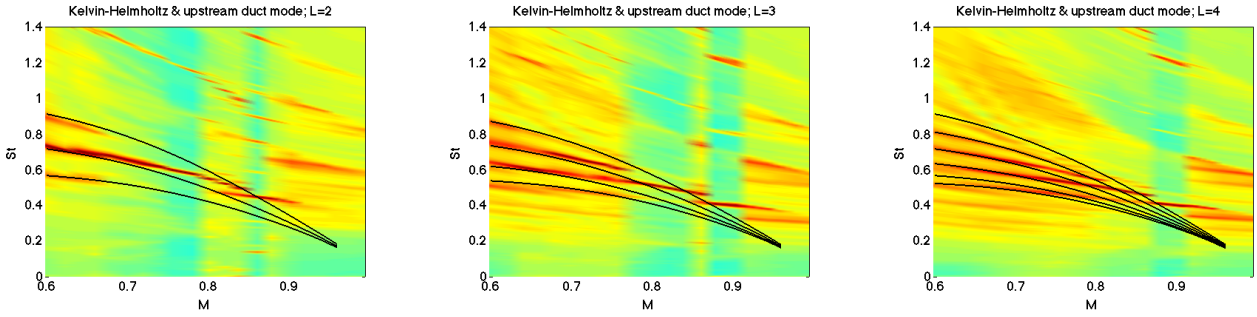


**Figure 8. Power spectral density measured by microphone, $p_{TW}$ (situated at $(x/D, r/D) = (0.04, 0.55)$) as a function of Mach number for jets with plate edge in the nearfield at (a) $x/D = 2$ (b) $x/D = 3$ and (c) $x/D = 4$. Plate edge is at $r/D = 0.5$ for all streamwise positions. Black lines show predictions based on resonance between the Kelvin-Helmholtz mode, $k^+_{KH}$, and the 'slow' trapped mode, $k^-_d$.**

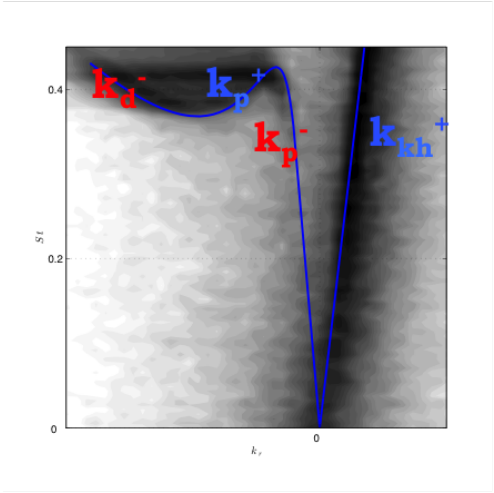


**Figure 9. Eigenvalue trajectories (dispersion relations) associated with the trapped waves and the Kelvin-Helmholtz modes superposed on a detail of the frequency-wavenumber spectrum shown in figure 1(b).**



Approximate expressions for the dispersion relations assocated with these modes are,

$$k_{KH}^{+} = \frac{\omega}{U_c}, \tag{4}$$

$$k_{p}^{-} = \frac{-\omega}{c}, \tag{5}$$

$$k_{p}^{+} = \frac{-\omega M + \sqrt{\omega^2 - \alpha^2(1-M^2)}}{1-M^2}, \tag{6}$$

$$k_{d}^{-} = \frac{-\omega M - \sqrt{\omega^2 - \alpha^2(1-M^2)}}{1-M^2}, \tag{7}$$

where $U_c$ is the convection velocity of the Kelvin-Helmholtz mode, $c$ the speed of sound, $M$ the jet Mach number and $\alpha$ the first root of the Bessel function, $J_0$; i.e. it corresponds to mode $(m, n_r) = (0, 1)$. If we consider the jet to behave like an open-ended duct of length $L$ (where $L$ is the streamwise position of the plate edge) that supports these modes, then resonance will occur when,

$$\Delta k = \frac{n\pi}{L} \qquad n = 1, 2, 3, \ldots, \tag{8}$$

in which case the resonant frequencies for the four resonance scenarios (any combination of a $k^+$ and $k^-$ wave), are,

$$\omega_{(k_{KH}^{+};k_{p}^{-})} = \frac{2n\pi c M_c}{L(c+M_c)}, \tag{9}$$

$$\omega_{(k_{KH}^{+};k_{d}^{-})} = \sqrt{\frac{4M_c^2(1-M^2)^2 n^2\pi^2 + \alpha^2 L^2 M_c^2 (1-M^2)}{L^2[(1-M^2)^2 + M^2 M_c^2 + M_c^2]}}, \tag{10}$$

$$\omega_{(k_{p}^{+};k_{p}^{-})} = \sqrt{\frac{4n^2\pi^2 c^2(1-M^2)^2 + c^2\alpha^2 L^2(1-M^2)}{L^2(c^2M^2 + c^2 + (1-M^2)^2)}}, \tag{11}$$

$$\omega_{(k_{p}^{+};k_{d}^{-})} = \sqrt{\alpha^2(1-M^2) + \frac{n^2\pi^2}{L^2}(1-M^2)^2}. \tag{12}$$

Comparison of these predictions with the observed peaks shows the following:

- The usual resonance scenario (equation 9) is clearly not responsible for the observed peaks, no correspondance being found between prediction and observation,
- The resonance scenario involving Kelvin-Helmholz wavepackets and the slow duct mode, $k_d^-$ (equation 10), shown in figure 9 by the black lines, captures the low Mach-number trend,
- At Mach numbers approaching and beyond $M = 0.82$ no clear match can be found between the hypothesised resonance scenarios and the data.

To further explore the mechanisms responsible for the high Mach number trend we replot the spectra in terms of Helmholtz number. An example is shown in figure 10 for plate-edge position, $x/D = 4$ and serves to illustrate a change in behaviour at about $M = 0.75$, which is where the low-Mach-number resonance mechanism identified in figure 10 ceases. Above this Mach number the peaks scale with Helmholtz number, implying that the phase speeds of the modes involved in the resonance are independent of the Mach number.

In addition to this, we note that the model used to compute the resonance scenario between $k_p^+$ and $k_p^-$ is the least precise of the four, as it does not take into account the shape of the dispersion relations near saddle point $S2$, as shown in figure 11(a), suggesting that the $k_p^+$ and $k_p^-$ modes near saddle point 2 may be those involved in the resonance.

The phase speed associated with saddle-point $S2$ provides a rough estimate of the phase speed of the $k_p^+$ ad $k_p^-$ modes near the saddle point. This is shown in figure 11 as a function of Mach number, and confirms that the change in phase speed is slight over the high Mach-number range. Given the Helmholz scaling observed, this leads us to posulate that the resonance mechanism in the high Mach number range is indeed underpinned by these modes. Verification will require exploration of the cylindrical vortex-sheet dispersion relation as a function of Mach number.

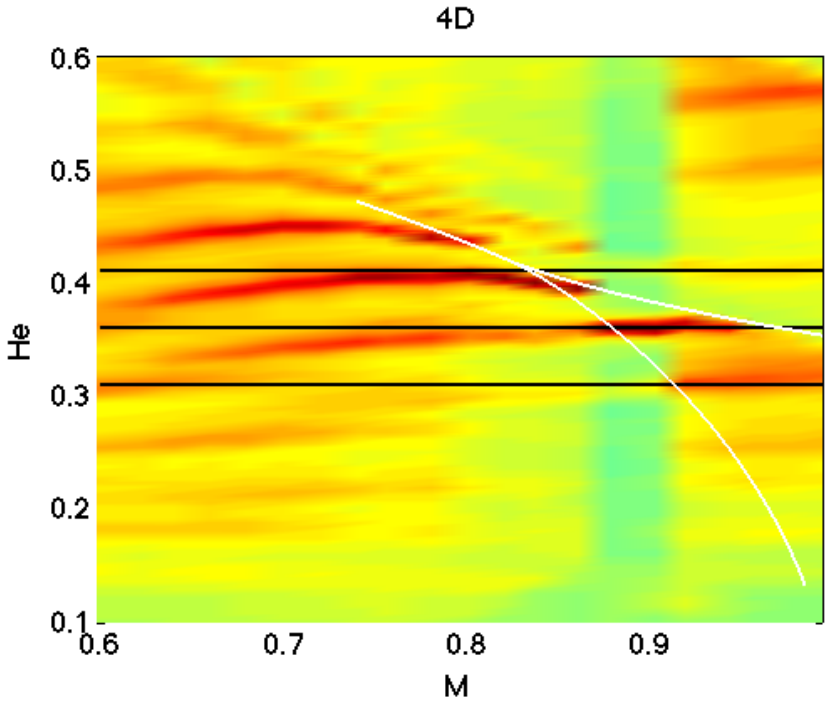


ccc

**Figure 10. Power spectral density in terms of Helmholtz number, $He = StM$. Lines of constant $He$ shown in black.**

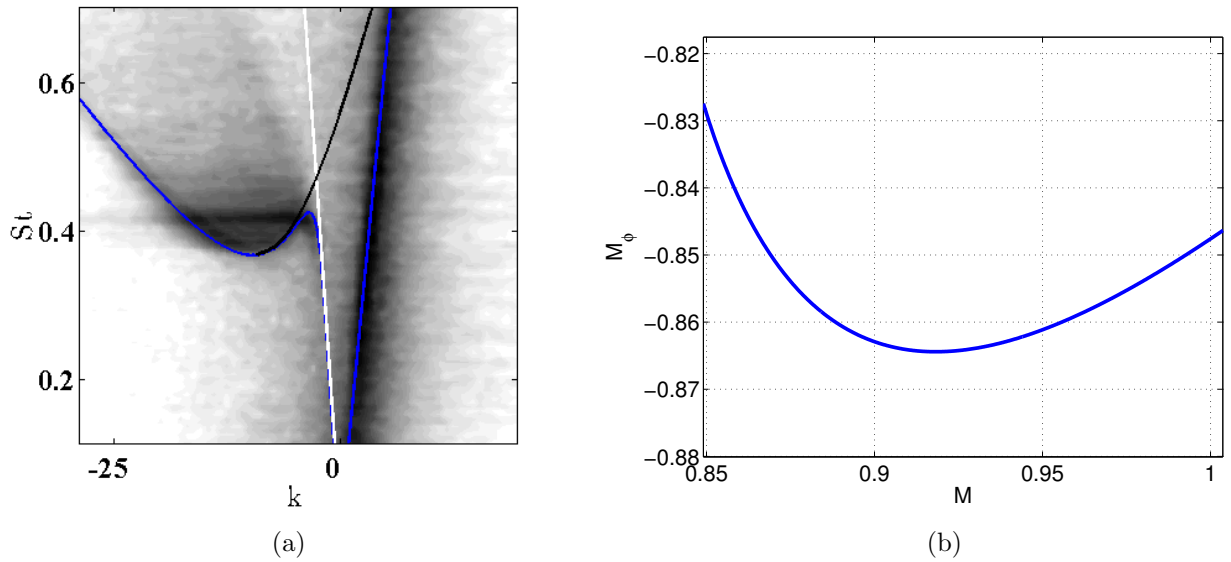


**Figure 11. (a) Approximate dispersion relations for $k_p^+$ (black line) and $k_p^-$ (white line); (b) phase speed associated with saddle-point $S2$ as a function of Mach number.**



## V. Conclusion

Tonal pressure fluctuations observed in the near-nozzle region of subsonic turbulent jets, explained in the studies of Towne *et al.*[13,14] and Schmidt *et al.*[11] as being due to acoustic modes trapped in the potential core, are found to radiate into the upstream arc. The experimentally identified Mach-number dependence of the tones shows that they occur over a Mach number range larger than that for which theory predicts propagative modes and neutral saddle points, suggesting that the modes are sustained by turbulent forcing even when evanescent. Stronger tonal dynamics and sound radiation (up to 170dB) occur when a sharp edge is situated in the nearfield of the jet. In the low Mach-number range ($M < 0.8$) these tones are shown to be due to a resonance involving convected hydrodynamic wavepackets and the 'slow', trapped acoustic mode. The trend observed in the Mach-number range, $0.8 \leq M \leq 1$, suggests that resonance is here driven by the 'fast' modes.

## References

[1]D. Breakey, P. Jordan, A.V.G. Cavalieri, O. Leon, M. Zhang, G. Lehnasch, T. Colonius, and D. Rodriguez. Near-field wavepackets and the far-field sound of a subsonic jet. In *19th AIAA/CEAS Aeroacoustics Conference*, 2013.

[2]G. A. Brès, V. Jaunet, M. Le Rallic, P. Jordan, T. Colonius, and S. K. Lele. Large eddy simulation for jet noise: the importance of getting the boundary layer right. In *21th AIAA/CEAS Aeroacoustics Conference*, 2015.

[3]G. A. Brès, P. Jordan, T. Colonius, M. Le Rallic, V. Jaunet, and S. K. Lele. Large eddys simulation of a mach 0.9 turbulent jet. In *Proceedings of the Center for Turbulence Research Summer Program, Stanford*, 2014.

[4]A. V. G. Cavalieri, P. Jordan, T. Colonius, and Y. Gervais. Axisymmetric superdirectivity in subsonic jets. *Journal of Fluid Mechanics*, 704:388, 2012.

[5]A. V. G. Cavalieri, D. Rodríguez, P. Jordan, T. Colonius, and Y. Gervais. Wavepackets in the velocity field of turbulent jets. *Journal of Fluid Mechanics*, 2012.

[6]A.V.G. Cavalieri, P. Jordan, W. Wolf, and Y. Gervais. Scattering of wavepackets by a flat plate in the vicinity of a turbulent jet. *Journal of sound and Vibration*, 333, 2014.

[7]P. Huerre and P. A. Monkewitz. Local and global instabilities in spatially developing flows. *Annual review of fluid mechanics*, 22(1):473–537, 1990.

[8]J. Lawrence and R. Self. Installed jet-flap impingement noise. In *Proceedings of the 21st AIAA/CEAS Aeroacoustics conference*, Dallas, TX, 2015. AIAA.

[9]A. Michalke. A note on the spatial jet instability of the compressible cylindrical vortex sheet. *Deutsche Luft- und Raumfahrt, DLR-FB 70-51*, 1970.

[10]S. Piantanida, V. Jaunet, J. Huber, W. Wolf, P. Jordan, and A.V.G. Cavalieri. Scattering of turbulent-jet wavepackets by a swept trailing edge. In *21th AIAA/CEAS Aeroacoustics Conference*, 2015.

[11]O. Schmidt, A. Towne, T. Colonius, A. V. G. Cavalieri, P. Jordan, and G. Brès. Trapped acoustic modes and linear

dynamics of a mach 0.9 turbulent jet: a global stability analysis. In *Proceedings of the 22st AIAA/CEAS Aeroacoustics conference*, Lyon, France, 2016. AIAA.

[12]T. Suzuki and T. Colonius. Instability waves in a subsonic round jet detected using a near-field phased microphone array. *Journal of Fluid Mechanics*, 565:197–226, 2006.

[13]A. Towne, A. V. G. Cavalieri, P. Jordan, T. Colonius, V. Jaunet, and G. Brès. Trapped waves in turbulent jets. In *Proceedings of the 6th Symposium on Global Flow Instability and Control*, Crete, Greece, 2015. Ercoftac.

[14]A. Towne, A. V. G. Cavalieri, P. Jordan, T. Colonius, V. Jaunet, O. Schmidt, and G. Brès. Acoustic waves in the potential core of jets. In *Proceedings of the 22st AIAA/CEAS Aeroacoustics conference*, Lyon, France, 2016. AIAA.

[15]K. B. M. Q. Zaman, A.F. Fagan, J.E. Bridges, and C.A. Brown. Investigating the feedback path in a jet-surface resonant interaction. In *Proceedings of the 21st AIAA/CEAS Aeroacoustics conference*, Dallas, TX, 2015. AIAA.